Available online at www.eccomasproceedia.org
Eccomas Proceedia COMPDYN (2025) 165-188

ECCOMAS
Proceedia

COMPDYN 2025
10th ECCOMAS Thematic Conference on
Computational Methods in Structural Dynamics and Earthquake Engineering
M. Papadrakakis, M. Fragiadakis (eds.)
Rhodes Island, Greece, 15-18 June 2025

A Spatio-Vectorial Graph Neural Network Model for Predicting Earthquake Intensity Measures (SV-MEIM) at Unsensored Locations

Ethan Ray[1], Jawad Fayaz[2]

[1]Graduate Student, Department of Computer Science, University of Exeter, Exeter, UK - er545@exeter.ac.uk

[2]Assistant Professor (Lecturer), Department of Computer Science, University of Exeter, Exeter, UK - j.fayaz@exeter.ac.uk

The spatially variable nature of earthquake ground motions cause localized structural damage and unpredictable structural responses near rupture zones. Whilst there are existing seismic sensor networks that record ground motions, these stations are too sparsely located to capture the shaking intensity variations between them accurately. This limitation directly complicates critical challenges such as rapid emergency coordination, region-specific infrastructure engineering, and targeted seismic risk reduction strategies. Since ground shaking cannot be directly measured at unsensored sites, this uncertainty creates significant risks for these priorities. To address this, intensity measures (IMs) at unsensored locations must be estimated through prediction or simulation. However, accurately modelling ground motion remains a complex challenge due to multiple barriers: (1) limited availability of reliable datasets; (2) gaps in existing seismic records due to uneven sensor coverage or data loss; (3) contamination of data by noise from non-seismic sources (e.g., human activity, equipment errors); and (4) the intricate, nonlinear relationships between interdependent physical variables governing seismic behaviour, such as soil properties, fault mechanics, and wave propagation dynamics. In this study, a graph neural network (GNN)-based model (called spatio-vectorial model for estimating earthquake IMs, SV-MEIM) is proposed to predict cross-dependent vector of ground motion IMs accounting for the spatial variability. In particular, GNN model consists graph attention (GAT) blocks along with multi-layer perceptron blocks. This spatial and vectorial regression is conducted via node-level regression of GNNs. In contrast to traditional ground motion models which do not take into account the spatial and cross IMs relationships, the GNN-based model offers a solution that estimates the vector of ground motion IMs across a regional area. The proposed model uses IMs such as spectral accelerations (S_a) from a network of stations and their site-specific characteristics like the average shear wave velocity in the top 30 metres of soil (V_{s30}) to predict IMs at sites without sensors. Node attributes include the IMs at sensor locations and their site-specific characteristics (like V_{s30}), while the edge attributes represent the spatial relationships, incorporating the differences between V_{s30} and polar distances between sites (this accounts for distances and relative angles). The node attributes are transformed using a novel exponential transformation to preserve the signs and scale of the values in the graph computations. The model is trained and validated using the next-generation attenuation (NGA) west-2 database of ground motion records. Statistical evaluations demonstrate that the GNN-based model achieves high predictive accuracy across multiple IMs and performs comparably to state-of-the-art methods. Notably, the GNN architecture requires less training data than conventional deep learning approaches, as node masking inherently reduces input dimensionality while maintaining predictive performance. The proposed SV-MEIM model enhances earthquake resilience by providing actionable tools for critical post-disaster priorities and long-term risk management. By delivering high-resolution shaking intensity

ISSN:2623-3347 © 2025 The Authors. Published by Eccomas Proceedia.
Peer-review under responsibility of the organizing committee of COMPDYN 2025.
doi: 10.7712/120125.12400.24583

estimates at unsensored locations, it enables rapid emergency response strategies—such as optimizing evacuation routes and prioritizing resource allocation. For infrastructure stakeholders, the model supports risk-informed decision-making by identifying buildings and lifelines (e.g., bridges, hospitals) most vulnerable to localized ground motion. The model further aids in generating high-fidelity shake maps for public alerts, insurance risk modelling, and recovery planning, collectively reducing economic losses and accelerating post-event recovery by minimizing downtime in critical systems.

1 Introduction

Earthquakes are natural geophysical phenomena resulting from the sudden release of energy along geological fault lines, typically occurring at tectonic plate boundaries [1]. These seismic events generate ground motion that varies spatially and temporally, with each event producing a distinct ground motion pattern from the rupture source [2, 3]. The severity of ground motion directly correlates with the extent of localized damage to infrastructure, human life, and economic systems in affected regions [4, 5].

To monitor and record seismic activity, global and regional seismic sensor networks have been established. These networks record the ground motion waveforms which are commonly quantitied through intensity measures (IMs) such as peak ground acceleration (PGA) and spectral acceleration (S_a) [6]. Despite their utility, the spatial distribution of these sensors is often sparse due to logistical, financial, and geographical constraints [7]. Consequently, there are significant gaps in data coverage, particularly in remote or densely populated urban areas where comprehensive seismic monitoring is critical [8]. These gaps hinder the ability to accurately capture the spatial variability of ground shaking during seismic events, limiting the effectiveness of early warning systems, emergency response planning, and seismic hazard assessments [9, 10].

From a public safety perspective, communities that are unaware of their seismic risk are more susceptible to loss of life and property during an earthquake [11, 10]. Structural failures in densely populated urban areas not only can lead to high casualty rates, but also result in long-term economic consequences hindering recovery efforts and placing additional strain on national resources [4, 12]. Implementing robust seismic hazard and risk models enhances the effectiveness of emergency services, facilitates risk-informed decision-making, and ultimately contributes to saving lives [13, 14].

Furthermore, the occurrence of secondary casualties, such as those caused by delayed rescue efforts or infrastructure failure, highlights the need for improved monitoring methods [8, 9]. While new seismic stations can be installed to cover unsensored areas, they are expensive to design, deploy, and maintain [15, 16], and are often susceptible to damage or destruction during large seismic events [17].

The most utilitarian alternative is to use the recordings from the existing sensor network and spatially propagate the shaking (quantified using IMs) through different models. Without an appropriate model, it is challenging to accurately determine the spatial distribution of IMs that correlate with the extent of damage in each area [18, 2]. Reliable implementations of such models can enable emergency response teams, infrastructure designers, and policy-makers to use the IM estimates for rapid decision-making and minimize potential damage and associated risks [19, 20].

Typically, ground shaking has been modelled through ground motion models (GMMs) also known as ground motion prediction equations (GMPEs). Early GMMs primarily relied on established statistical regression techniques to develop empirical relationships between the source and site parameters and the ground motion intensity at the site [21, 19, 22, 23, 24]. The GMMs are developed using historical earthquake records to estimate IMs such as PGA and S_a with input parameters such as moment magnitude (M), closest rupture distance (R_{rup}), soil's average shear wave velocity (V_{s30}), and others. Despite their computational efficiency and widespread use in probabilistic seismic hazard analysis (PSHA) [25], traditional GMMs face several inherent challenges. One of the most significant limitations is their reliance on predefined forms and the inability to effectively capture complex non-linear relationships that arise in ground shaking processes [19, 26]. Furthermore, these models often neglect explicit spatial correlation modelling between the sensor locations, thereby providing independent predictions for each site without accounting for the spatial dependency of ground motions [27]. This limitation can lead to inaccuracies, especially when modelling regional ground motion fields [20].

The emergence of machine learning has revitalized research in ground motion modelling, leading to the development of deep learning-based generalized ground motion models (GGMMs) [28, 29, 30]. Unlike traditional GMMs, GGMMs leverage deep neural networks to capture complex, non-linear relationships inherent in ground motion IMs. These models utilize large-scale mathematical representations, allowing them to fit intricate patterns in IMs recorded by seismic sensors, which naturally exhibit non-linear dependencies with predictor variables such as M, R_{rup}, and V_{s30} [28].

Consequently, numerous specialized neural network architectures have been proposed to advance this field [31, 32, 33, 34, 35, 36]. For example, Fayaz et al. (2021, 2023) introduced a deep learning-based GGMM that employs a recurrent neural network (RNN) framework to simultaneously predict multiple IMs [37, 38]. Their approach integrates long short-term memory (LSTM) units to effectively capture complex sequential dependencies within the vector of amplitude-, duration-, frequency-, and energy- based IMs while preserving cross-IM correlations.

However, despite these advances, these GGMM do not incorporate spatial dependencies, restricting its predictive capabilities to existing sensor locations without providing estimates for unsensored areas. This limitation highlights the need for models that can integrate both temporal and spatial information to fully capture the spatial variability of ground motions [13, 32].

Another approach by TISER-GCN [39] constructs a graph from seismic waveforms using convolutional neural network (CNN) layers. This graph-based model leverages graph convolutional networks (GCNs) to capture spatial relationships and dependencies between seismic stations. However, this CNN-based transformation operates as a "black-box," offering limited interpretability regarding how the graph structure is derived from the waveform data. This lack of transparency raises concerns about the robustness and generalizability of the model, particularly when applied to diverse seismic environments. Furthermore, the model is constrained to predicting only five IMs per node, which restricts its applicability for comprehensive seismic hazard assessments. Another limitation of the study includes that it doesn't test the predictive performance through absolute evaluation metrics such as the coefficient of determination (R^2) The omission of these evaluation tools limits the model's ability to be systematically compared against other approaches and hinders its usability in practical decision-making contexts.

Other spatial-based models, such as Zhang et al. [40], leverage spatio-temporal graph structures to enhance prediction accuracy, however they do not predict IMs but rather aim to predict the longitude, latitude, depth and M of the earthquake event. Whilst this can be useful for classifying earthquakes, it does not present the inherent response during ground shaking.

In this study, a novel spatio-vectorial model, termed SV-MEIM (spatio-vectorial model for estimating earthquake intensity measures) is proposed. SV-MEIM leverages graph neural networks (GNNs), specifically graph attention networks (GATs), for the spatial prediction of ground motion IMs. SV-MEIM explicitly integrates spatial dependencies by representing seismic stations and their interactions as a graph structure. The model applies GATs to dynamically assign adaptive attention weights to neighbouring nodes, allowing it to selectively focus on the most relevant seismic stations and mitigate noise from less informative connections [41]. Furthermore, GATs excel in irregular, non-Euclidean domains by dynamically weighting station interactions based on learned importance, improving robustness against missing or imbalanced data. Additionally, the study proposes a novel transformation for IMs to effectively stabilizes the lognormal nature of IMs and preserve signs and scale to inherent the physics of the IMs in graph computations.

The SV-MEIM framework extends beyond traditional approaches by incorporating a vectorial representation of IMs, PGA and spectral acceleration (S_a) at various periods, alongside site characteristics and inter-station distances. This enables the model to jointly learn spatial correlations and cross-IM dependencies, providing a more comprehensive understanding of seismic event dynamics. Additionally, by formulating seismic data as a graph learning problem, SV-MEIM is capable of estimating IMs at unsensored locations, effectively increasing the spatial granularity of hazard predictions. The proposed approach is particularly advantageous in real-world seismic networks, where station coverage is often sparse and geographically uneven.

By integrating physics-based principles with machine learning, SV-MEIM advances earthquake rapid response models and seismic hazard assessment. Its ability to estimate spatial IMs across large regions contributes to reducing uncertainty in hazard prediction, thereby enhancing early warning systems, infrastructure resilience planning, and post-earthquake recovery efforts. Ultimately, SV-MEIM aims to minimize economic losses and casualties, supporting more effective disaster response strategies and improving seismic resilience at both local and regional scales.

2 Conceptualisation

Modelling seismic networks through graph theory offers an effective means of capturing the spatial dependencies inherent in ground motion IMs. In this study, the seismic network is conceptualized as an undirected weighted graph $G = (V, E, A)$, where V represents the set of nodes (seismic stations), E denotes the set of edges (spatial relationships between stations), and A is the adjacency matrix encoding the connectivity and strength of the relationships.

2.1 Graph Construction

Each seismic station is represented as a node $v_i \in V$. Connections (edges) between nodes are established based on the geographical proximity of the stations, ensuring that the graph structure reflects real-world spatial relationships. To quantify the distance between stations, the Haversine formula is employed [42]. Unlike the Euclidean distance, the Haversine distance accounts for Earth's curvature, which is essential when dealing with regional or global seismic networks. The Haversine distance is expressed in Equation (1), where d is the great-circle distance between two stations, r is Earth's radius (approximately 6371 km), θ_1 and θ_2 are the latitudes of the two stations (in radians), $\Delta\theta = \theta_2 - \theta_1$ is the latitude difference, and $\Delta\lambda = \lambda_2 - \lambda_1$ is the longitude difference.

$$d = 2r \arcsin\left(\sqrt{\sin^2\left(\frac{\Delta\theta}{2}\right) + \cos(\theta_1)\cos(\theta_2)\sin^2\left(\frac{\Delta\lambda}{2}\right)}\right), \tag{1}$$

2.2 Node Attributes

Each node in the graph is associated with a feature vector $\mathbf{x}_i$ that encapsulates site-specific parameters and IMs. These features enable the model to learn localized and regional seismic patterns. The following parameters reflect the node attributes:

- **Geographic location:** Latitude and longitude of the coordinates of the stations provide an essential spatial context.
- **Seismic IMs:** IMs of ground motions recorded at the various stations for a given earthquake event such as S_a at various periods and PGA.
- **Site characteristics:** Parameters that characterize local site effects on seismic waves, such as V_{s30}.

These attributes allow the model to learn both localised and regional seismic patterns. The attributes much be transformed through an appropriate transformation (T_r) to: (1) preserve the inherent differences in scale between the IMs while ensuring meaningful learning representations, and (2) prevent interference in the internal graph convolutions that could arise if the natural logarithm were used, potentially introducing opposite-signed values within the node feature vectors.

2.3 Edge Attributes

Edges are enriched with features that capture inter-station relationships and geophysical dependencies. The edge feature vector $\mathbf{e}_{ij}$ between the nodes v_i and v_j include:

- **Distance:** The Haversine distance computed between stations provides a primary measure of spatial separation.
- **Seismic correlation:** Cosine similarity between IM vector, reflecting the degree of ground motion similarity.
- **Site condition differences:** Differences in V_{s30} values between stations, indicating potential variations in local amplification effects.

Since the ground motion amplitude attenuates as the station is farther from the seismic source/hypocentre, edges are established between nodes only if the calculated distance d falls below a predefined threshold. In this study, this threshold is calculated as the mean distance between stations plus one standard deviation.

The process of transforming the data into a graph representation is summarized in Figure 1.The details of the T_r are described in Section 4.2. This graph representation enables the application of GNNs and other graph-based learning methods to extract meaningful spatial dependencies from the resulting graph.

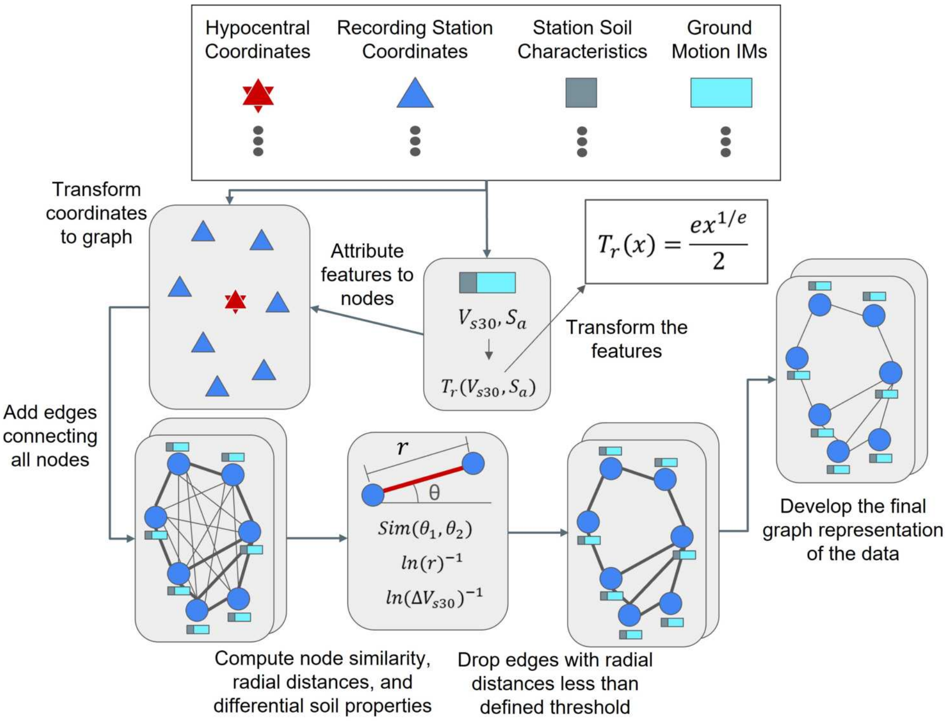

Figure 1: Process of constructing graph representation from the seismic data

3 Database

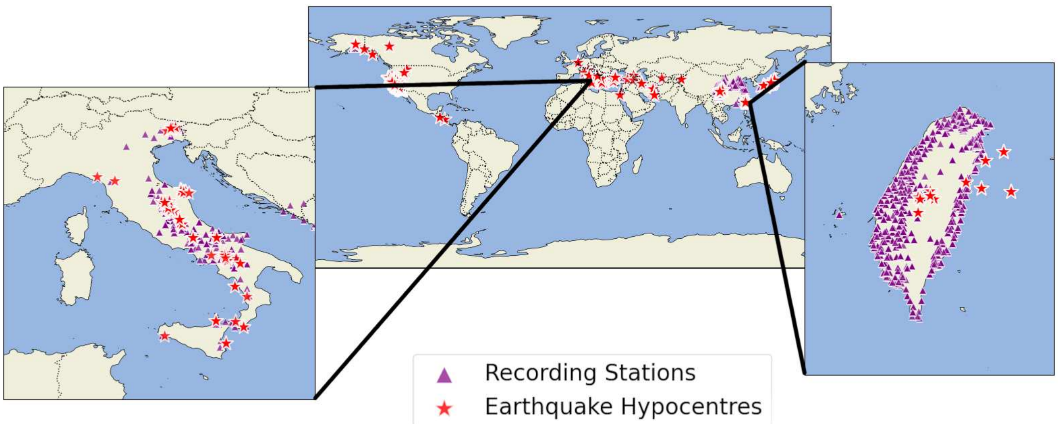

Figure 2: Geographic representation of NGA-west2 database; Italy (left), and Taiwan (right)

This study utilizes the next generation attenuation (NGA)-west2 database [43], which comprises 21,336 ground motion records from 599 seismic events worldwide (Figure 2). Developed as an update to the original NGA-west project [44], NGA-west2 expands the range of recorded earthquakes, incorporating data from recent large-magnitude events and diverse tectonic settings. The dataset includes 8337 events recorded from 91 earthquakes with M >5; ground motions from various faulting mechanisms strike-slip (12597 records), reverse (5085 records), and normal (606 records) captured across a wide spectrum of site conditions, from soft soils (9931 records at $V_{s30} < 400$ m/s), to dense soils (10652 records at $400 < V_{s30} < 800$ m/s) to stiff rock (753 records at $V_{s30} > 800$ m/s).

The S_a spectra of the ground motions with PGA >0.05g in the NGA-west2 database are presented in Figure 3(a). In particular, the RotD50 definition of S_a is utilized as the IM in this study [45]. Unlike other definitions (such as geomean, average, etc.), RotD50 S_a is independent of the orientation of the recording sensor and leads to the one-to-one causal relation between the source parameters and spectral acceleration. As observed from the figure, the spectra of the selected ground motion represent both low levels of shaking ($S_a <$ 0.1 g) and high levels of shaking ($S_a >$ 0.5 g).

Since the modelling of spatial dependencies require multiple earthquake events to be recorded at multiple stations, a subset of this data was taken to train the SV-MEIM model. This is done by computing a bipartite graph linking stations to common earthquake events and then selecting the bipartite graph which contains the most seismic events recorded across all common stations. Filters are applied to each bipartite graph such as the number of stations > 20 and the number of common earthquakes > 5.The S_a spectra of the selected subset of ground motions are presented in Figure 3(b)

While alternative datasets could be used to follow the same modelling process outlined in this paper, NGA-west2's comprehensive coverage and standardized format makes it the preferred choice for this study.

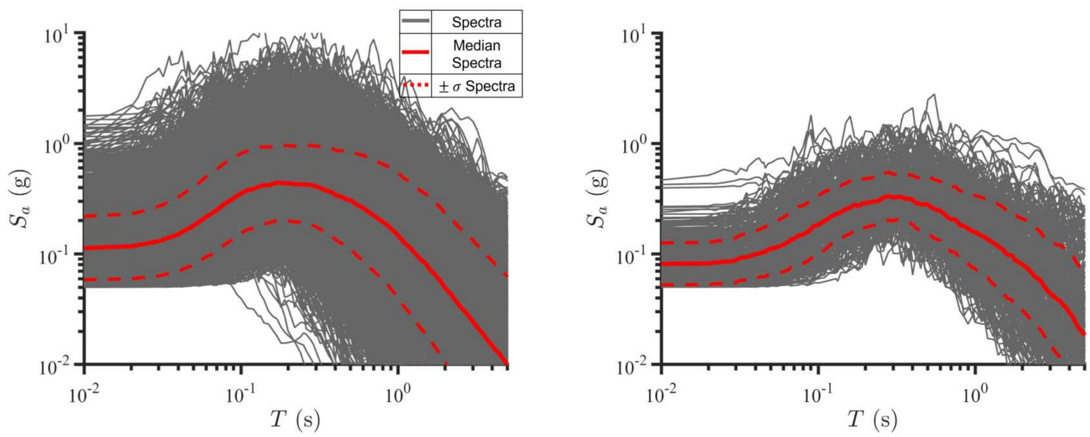

(a) (b)

Figure 3: (a) S_a spectra of NGA-west2 ground motions; (b) S_a spectra of selected subset of ground motions

4 Method

To model and predict ground motion IMs, a GNN is developed to capture the spatial dependencies between seismic stations during earthquake events. The data is structured as a bipartite graph, where edges represent connections between seismic stations and recorded seismic events, enabling the model to learn the spatial relationships that govern ground motion propagation. The methodology comprises multiple stages, including data preprocessing, graph construction, and neural network design, each optimized to enhance predictive accuracy.

4.1 Bipartite Representation

The interaction between seismic stations and recorded earthquake events is formulated as a bipartite graph, where stations are connected through multiple shared seismic events. This structure allows the representation of spatial dependencies in ground motion IMs while preserving the relationships between recording stations and seismic sources. Multiple instances of this bipartite graph can be constructed for regions with sufficient seismic data, enabling a standardized and transferable framework applicable across different geographic locations worldwide.

Figure 4 illustrates the formation of this bipartite graph on a three-dimensional plane. The visualization incorporates terrain elevation, represented using a colour gradient, to provide geographic context for the spatial distribution of seismic activity. By structuring seismic networks in this manner, the model can analyse shared seismic events across stations, enhancing its ability to generalize to new regions and improving the robustness of seismic network studies globally.

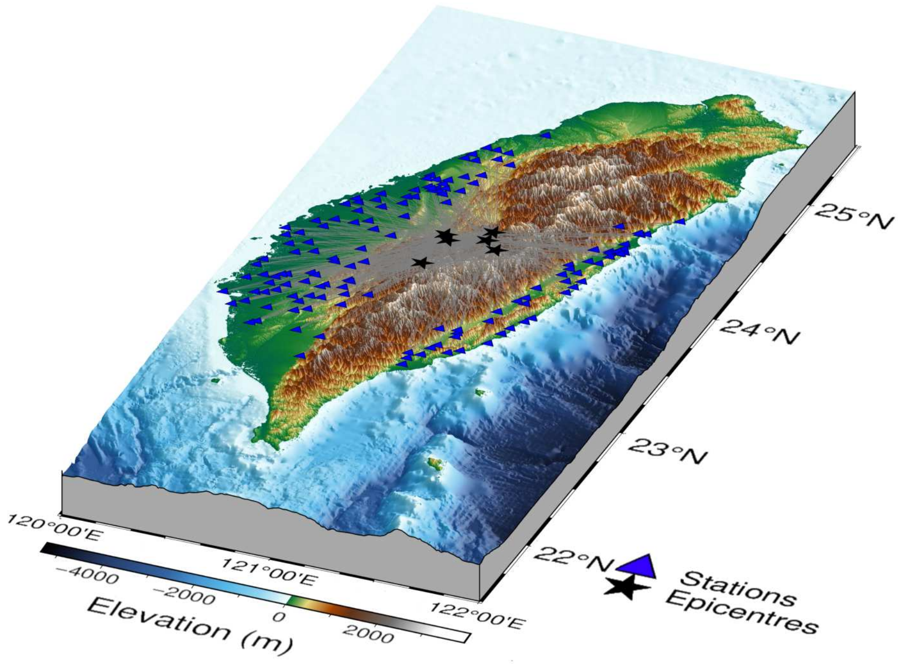

Figure 4: Taiwan's terrain overlaid with a bipartite graph connecting recording stations (blue triangles) and earthquake epicentres (black stars)

Once the associations between seismic stations and recorded earthquake events are established, the data is preprocessed to ensure compatibility with graph-based analysis. Each node in the graph represents a seismic station and is assigned site-specific features, including station coordinates (longitude, latitude), PGA, S_a, V_{s30}, and other relevant IMs. The edges connecting nodes encode the relationships between seismic events and the stations that recorded them. These relationships are weighted based on multiple factors, such as geographic proximity (i.e., distance between stations) and difference in site-specific soil conditions (i.e. difference in V_{s30}), allowing the model to account for both spatial dependencies and the correlation of seismic wave propagation.

The station data and corresponding IMs are integrated into a feature matrix $\mathbf{X} \in \mathbb{R}^{N \times F}$, where each row represents a station-event pair, with N being the number of nodes and F the number of features. This matrix serves as input for constructing the graph, with edges linking stations to seismic events, ensuring that the model learns from shared data relationships. The structured representation of seismic IMs in a bipartite graph provides a systematic framework for training the graph-based neural network.

To optimize the bipartite representation, the focus is placed on retaining the most informative data while eliminating redundant or irrelevant features. Feature selection is applied to reduce model complexity and enhance computational efficiency. Specifically, only key features such as PGA, S_a, V_{s30}, and station coordinates are retained. This selection ensures that the model is trained on the most critical parameters, minimizing overfitting and improving generalization while maintaining computational efficiency.

4.2 Custom Transformation

S_a of ground motions is typically modelled as a lognormal distribution [22, 46]. However, the implementation of GNNs requires expanding the node attribute vector by incorporating the edge attribute vector, ensuring that distances remain continuous across all states. This necessitates a transformation that preserves positivity and maintains scale differences across attributes.

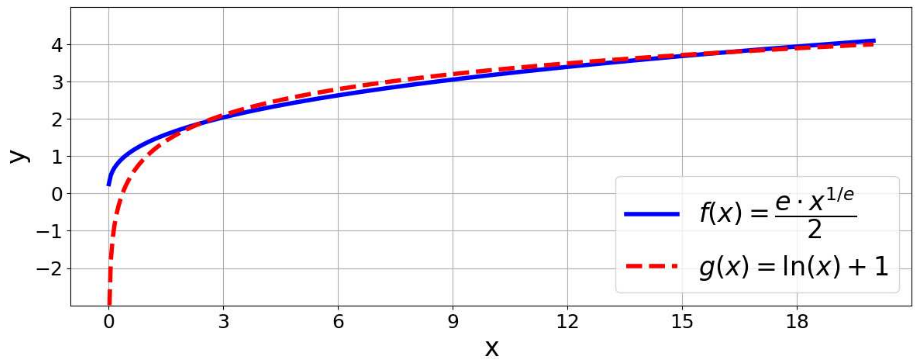

Figure 5: Comparison of $T_r(x)$ vs. natural log transformations

To achieve this, a transformation $T_r(x)$ expressed in Equation (2) is applied. This transformation modifies the input x using a fractional power, scaling, and normalization. This offers several advantages over conventional approaches such as the natural logarithm. The exponent e^{-1} smooths variations by suppressing large values while enhancing smaller ones, making it particularly effective for handling data with a wide range of magnitudes. The multiplication by e amplifies the transformed values, while the division by 2 prevents excessive growth. Additionally, unlike the natural logarithm, $T_r(x)$ is sign-preserving, ensuring that values remain positive and continuous even for inputs below 1. This property is crucial for preserving the physics of the problem in models like SV-MEIM, where discontinuities in attribute scaling could disrupt the continuity of spatial relationships. Figure 5 presents a comparison of $T_r(x)$ against the natural logarithm.

$$T_r(x) = \frac{ex^{\frac{1}{e}}}{2} \tag{2}$$

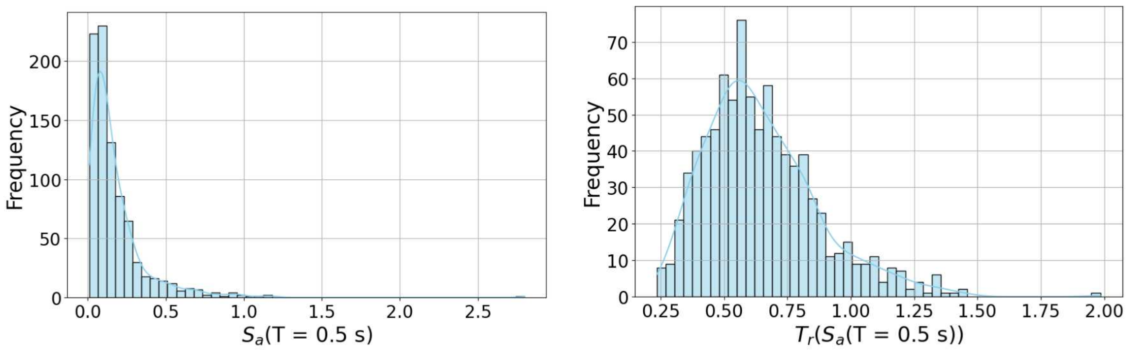

(a) (b)

Figure 6: Comparison of the (a) original and (b) transformed distributions of S_a at T =0.5s

The results of this transformation, $T_r(x)$, are shown in Figure 6. As shown, $T_r(x)$ effectively converts an exponentially distributed data of S_a into a normal distribution, maintaining the consistency necessary for stable and accurate model training.

4.3 Graph Representation

Graphs provide an effective framework for modelling problems that involve complex, non-linear relationships between entities. In the context of ground motion IM prediction, a graph-based approach allows for the explicit representation of spatial and vectorial dependencies between seismic events and recording stations. By structuring the data as a bipartite graph—where seismic stations and earthquake events serve as nodes, and relationships between them are encoded as edges—shared event-station interactions are captured. This structured representation enables the model to learn spatial dependencies that are often overlooked in traditional ground motion models [47].

One of the key advantages of using a graph-based representation is its ability to efficiently process large, unstructured seismic datasets by explicitly modelling spatial dependencies between stations rather than treating observations as independent samples. Unlike traditional machine learning approaches, which assume independent and identically distributed (i.i.d.) data, the graph structure preserves inter-station relationships, allowing the model to learn the spatial correlation of seismic waves [48].

By leveraging the adjacency matrix and node feature matrix, the graph-based model aggregates information across connected stations, effectively capturing spatial patterns in ground motion propagation. GNNs utilize these relationships and incorporate both local and global spatial dependencies. Furthermore, GNNs are particularly well-suited for this type of data due to their ability to operate on irregular, non-Euclidean domains, making them highly effective in handling the spatial sparsity and heterogeneous station distribution that characterizes real-world seismic networks [49].

To accurately represent the spatial relationships in earthquake data, the use of polar coordinates is particularly advantageous. Since seismic waves propagate radially outward from their epicentre, modelling spatial dependencies in polar coordinates provides a more natural and interpretable framework for capturing distance-dependent wave propagation patterns. The conversion from Cartesian to polar coordinates is performed using the standard transformation, Equations (3) to (6), where r represents the radial distance from a central reference point (computed as the centroid of station locations), and φ denotes the azimuthal angle [50].

$$x = r \cdot \cos(\varphi), \tag{3}$$

$$y = r \cdot \sin(\varphi), \tag{4}$$

$$r = \sqrt{x^2 + y^2}, \tag{5}$$

$$\varphi = \text{atan2}(y, x). \tag{6}$$

This transformation provides a more structured representation of seismic wave propagation, simplifying the learning process for the graph-based neural network. Additionally, by expressing station relationships in polar coordinates, the model can efficiently compute great-circle distances using the Haversine formula (refer to Figure 1 in the Conceptualization section), further enhancing its ability to capture spatial dependencies in seismic wave propagation.

4.3.1 Connections

The computed radial distance r is used to determine connectivity between nodes. A connection between two nodes is established if $r < d$, where d is defined as the average inter-node distance plus one standard deviation. This threshold ensures that most nodes maintain sufficient connections to facilitate effective learning. However, in cases where a node fails to establish at least three neighbouring connections, the k-nearest neighbours (KNN) algorithm is applied to guarantee a minimum level of connectivity [51].

The graph is represented as a weighted directed network [52, 53], where edges encode the relationships between seismic stations based on their recordings of shared seismic events. This structure is commonly used in graph-based earthquake models [39, 40, 54]. Each edge transmits information regarding the proximity of stations, IMs of ground shaking, and the shared characteristics of both the stations and seismic events. The direction of edges is assigned based on the data flow, typically oriented from one station to another, ensuring that information is propagated in a manner consistent with the predictive framework.

The weighting of the edges reflects the strength of these relationships, with higher weights assigned to stations exhibiting greater similarity in ground motion characteristics. Directionality plays a crucial role in model prediction, as information should flow from known stations to unknown locations, maintaining bidirectional relationships only where data availability permits. This structured approach allows the model to effectively capture spatial dependencies, enabling it to learn how seismic waves propagate across different regions and how ground motion intensity varies across geographical locations.

4.3.2 Edge Weights

The edges in the graph are assigned multi-dimensional weights that capture the spatial and geophysical relationships between stations. Since the system is represented in Polar coordinates, edge weights incorporate both the r between two stations and the similarity of φ. Additionally, the inverse of the absolute difference in Haversine distances between stations is used to emphasize the influence of stations closer to the target stations. Stations located farther from the target station receive lower weights, reflecting their diminished impact on ground motion observations at the target location.

To account for variations in local site conditions, the difference of V_{s30} values between connected stations is also included as an edge weight. This feature helps quantify the effect of soil properties on seismic wave propagation.

By integrating these weighted relationships, the model effectively captures spatial dependencies in ground motion IMs, enhancing its ability to predict seismic intensity at locations where direct recordings may be unavailable.

4.3.3 Node Weights

Node weights encode intrinsic properties of seismic stations and earthquake events, independent of the connections (edges) between them. For stations, these weights capture site-specific factors influencing ground motion, such as local soil conditions, seismic amplification, and geological properties. Key features selected for this model include PGA, V_{s30}, and S_a, all of which undergo transformation of Equation (2) to ensure consistency across the dataset.

These weights allow the model to differentiate between stations based on their ability to capture seismic signals accurately. For instance, stations on soft soils typically record more intense ground shaking than those on hard rock, even at the same epicentral distance [55, 56]. Encoding such variations as node weights enables the model to assign greater importance to stations that provide more representative seismic measurements.

Other earthquake-specific characteristics could be used for node weights, for example magnitude and depth of the event could be utilised, however they are determined days after the seismic event [57]. While these factors directly affect the intensity of ground motion recorded at each station, the SV-MEIM model is currently designed as a rapid response model. Hence, only the key features which are available during and right after the event are used in training the model.

4.4 SV-MEIM Model Architecture

The SV-MEIM model utilizes a GNN framework to estimate missing or extrapolate S_a values based on connectivity and shared information among seismic stations. The architecture follows a structured pipeline consisting of three primary stages: input graph construction, feature propagation via GAT layers, and prediction refinement using a multi-layer perceptron (MLP). Figure 7 illustrates the complete model workflow.

The input graph is constructed with seismic stations as nodes, each characterized by site-specific parameters. Target stations, where S_a needs to be inferred, are denoted in orange, while known stations providing observations are shown in blue. The graph structure encodes spatial dependencies through weighted edges, where relationships are defined based on proximity, geological similarity, and inter-station correlations. The inclusion of directional and bidirectional edges ensures that asymmetric and symmetric dependencies in seismic IM propagation are effectively captured. Each node is assigned an attribute vector consisting of

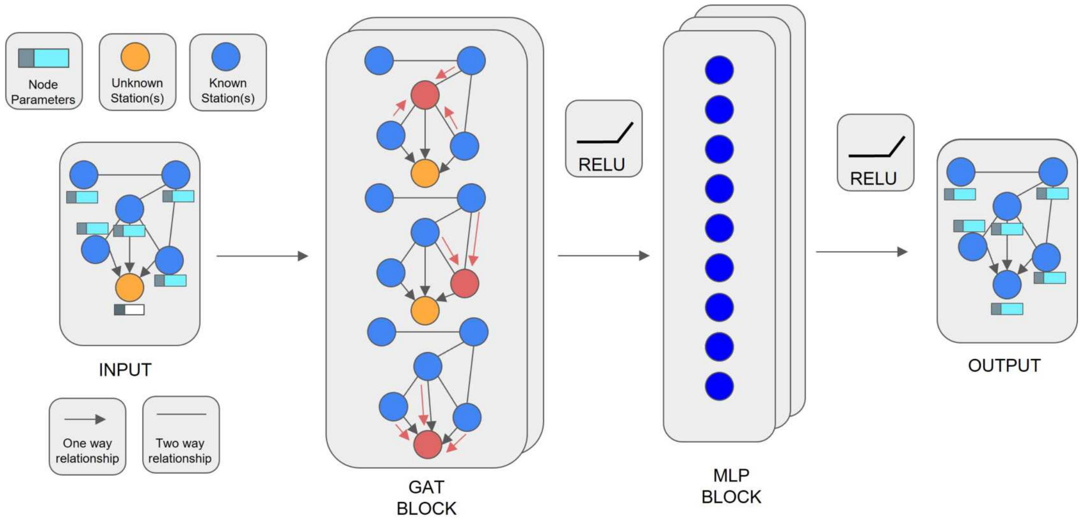

Figure 7: SV-MEIM model architecture. The input graph consists of seismic stations (nodes) with associated parameters. Unknown stations (orange) represent target sites for inference. The GNN propagates information through GAT layers, followed by dense MLP layers with ReLU activation, before reconstructing the inferred node values in the output graph

known station parameters such as PGA, S_a, and V_{s30}, while edge attributes encode spatial correlations and site conditions.

In the feature propagation stage, GAT layers iteratively refine node embeddings by aggregating information from neighbouring stations through attention-weighted message passing. This mechanism allows the model to prioritize influential stations while suppressing less relevant connections. The feature update at each node is governed by the Equation (7) where the attention coefficient $\alpha_{i,j}$ is computed as Equation (8). In these equations, $\mathbf{x}_i$ represents the feature vector of node i, $\mathbf{\Theta}$ are trainable weight matrices, and $\mathbf{e}_{i,j}$ encodes edge attributes. This attention mechanism ensures that the model dynamically adjusts the importance of different stations based on their contribution to the prediction.

$$\mathbf{x}'_i = \sum_{j \in \mathcal{N}(i) \cup \{i\}} \alpha_{i,j} \mathbf{\Theta}_t \mathbf{x}_j, \tag{7}$$

$$\alpha_{i,j} = \frac{\exp\left(\text{LeakyReLU}\left(\mathbf{a}_s^\top \mathbf{\Theta}_s \mathbf{x}_i + \mathbf{a}_t^\top \mathbf{\Theta}_t \mathbf{x}_j + \mathbf{a}_e^\top \mathbf{\Theta}_e \mathbf{e}_{i,j}\right)\right)}{\sum_{k \in \mathcal{N}(i) \cup \{i\}} \exp\left(\text{LeakyReLU}\left(\mathbf{a}_s^\top \mathbf{\Theta}_s \mathbf{x}_i + \mathbf{a}_t^\top \mathbf{\Theta}_t \mathbf{x}_k + \mathbf{a}_e^\top \mathbf{\Theta}_e \mathbf{e}_{i,k}\right)\right)}. \tag{8}$$

Following the GAT layers, the learned node embeddings are processed through an MLP block, which refines the predictions before reconstructing the inferred node values in the output graph. The MLP consists of fully connected layers with ReLU activation functions, which introduce non-linearity and enhance feature representation. The final output includes predicted PGA and S_a values for the target stations, generating a completed seismic network representation that integrates both observed and inferred values.

Beyond spatial relationships, the model incorporates temporal dependencies to capture dynamic variations in ground motion IMs. Spatio-temporal extensions [58, 59] leverage sequential modelling techniques to track vectorial modelling of IMs. Transformer-based mechanisms and recurrent layers are applied to encode vector-representation of IMs while preserving spatial structure, improving predictive accuracy in real-world applications.

By integrating attention-based learning and spatio-vectorial modelling, the SV-MEIM model provides a robust framework for predicting seismic IMs at target stations with missing sensors/data. The combination of GAT layers for spatial feature extraction and MLP layers for final inference ensures that the model can effectively generalize across regions with diverse seismic conditions.

5 Results and Discussions

This section discusses the training performance and evaluates the predictive power of the SV-MEIM model. The section further conducts a residual analysis of the model and then implements a case study on Taiwan to assess it's spatial predictions against the available data.

5.1 Training Performance and General Evaluation

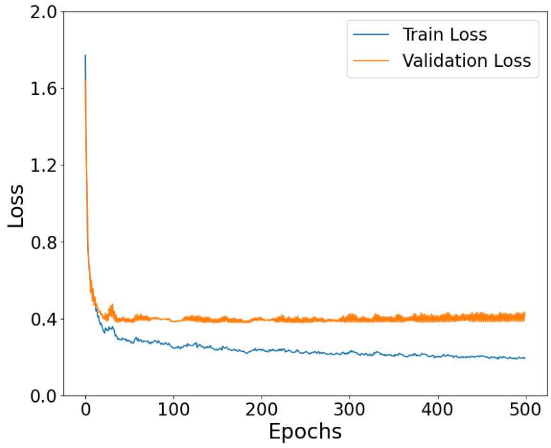

(a)

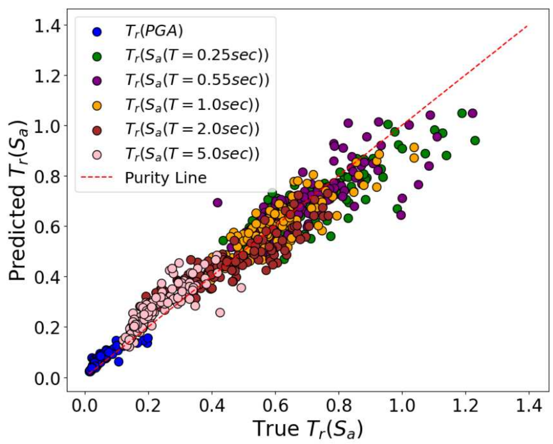

(b)

Figure 8: (a) Train and validation losses over epochs; (b) True vs predicted $T_r(S_a)$ (purity plot)

To assess the model's training efficiency and its ability to generalize, loss curves are analysed over the 500 training epochs, as illustrated in Figure 8(a). The validation set comprises 20% of randomly selected stations (i.e., validation set), which are entirely withheld from training to evaluate the model's ability to infer PGA and S_a values at unseen locations.

The loss plot reveals an initial sharp decline in both training and validation loss, indicating rapid convergence in the early training phase. As training progresses, the training loss continues to decrease, whereas the validation loss stabilizes at a relatively higher level, suggesting that while the model effectively minimizes error on the training set, some degree of overfitting occurs over extended epochs. Despite this, the validation loss remains consistently low, demonstrating that the model retains strong generalization capabilities across different seismic stations.

Figure 8(b) displays the purity plot, which visualizes how the true $T_r(S_a)$ compares to the predicted $T_r(S_a)$ across multiple periods. A strong alignment along the diagonal reference line (dashed red) indicates that the model's predictions closely approximate the actual values. However, slight deviations are observed for certain spectral periods, particularly for lower-period S_a values (e.g., 0.25s and 0.55s), where a greater spread is evident. This suggests that shorter-period ground motions exhibit increased variability. This is in line with the past studies that have demonstrated the difficulties in modelling the high frequency domain of ground motions [60, 61].

5.2 Model Performance Across Periods

Figure 9 presents the R^2 values for both training and validation sets across different periods, providing key insights into the model's predictive performance and generalization capabilities. A higher R^2 value suggests that the model effectively captures variance in the dataset, leading to more accurate predictions. In this case, the training scores demonstrate strong performance, particularly for mid and long periods ($T > 0.5s$), indicating that the model successfully learns mid-to-low frequency characteristics. The validation R^2 values, while exhibiting more variability, closely follow the training scores, suggesting that the model generalizes well across different seismic stations.

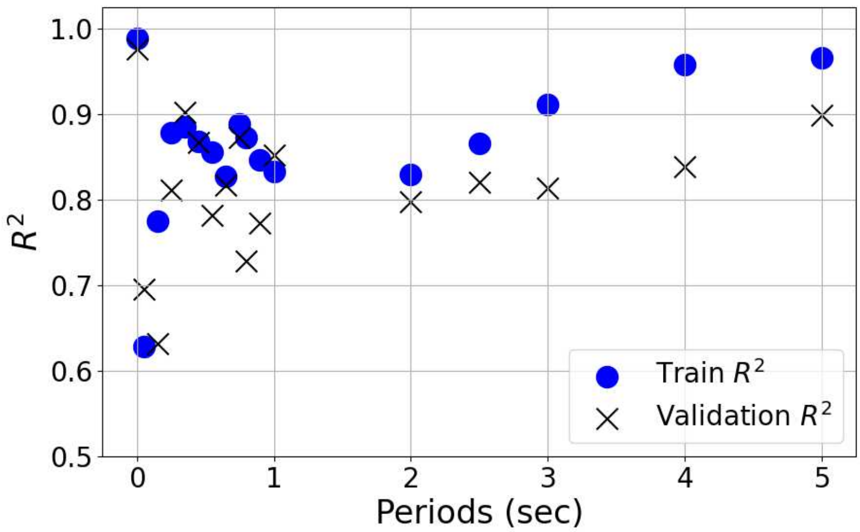

Figure 9: R^2 values for train and validation sets

A notable observation is the model's performance at $T = 0s$ (i.e., PGA), where it achieves a high R^2 value, indicating strong predictive capability. The R^2 drops for short periods close to $T = 0.1s$, however, increase right after $T = 0.2s$. This suggests that the model is moderately well-suited for estimating mid-to-high frequency of ground motions, which are crucial for understanding the response of smaller structures and low-rise buildings that are sensitive to short-period oscillations.

However, at very short periods ($T = 0.05s$ and $T = 0.015s$), the R^2 values exhibit a significant drop, indicating lower predictive accuracy. This decline is likely attributed to the increased signal noise and local site effects that heavily influence high-frequency ground motions, making them more challenging to model accurately.

For longer spectral periods ($T > 2s$), the model maintains consistently high R^2 values in both training and validation sets, indicating reliable performance for predicting ground motions associated with larger structures and flexible buildings. The strong alignment between training and validation scores in this range suggests that the model effectively captures long-period ground motion characteristics with minimal overfitting. These findings reinforce the SV-MEIM's robust generalization ability while also identifying specific spectral ranges where improvements can be made. By addressing the observed limitations at very short spectral periods, the model's applicability to real-world seismic risk assessments can be further improved.

5.3 Residual Analysis

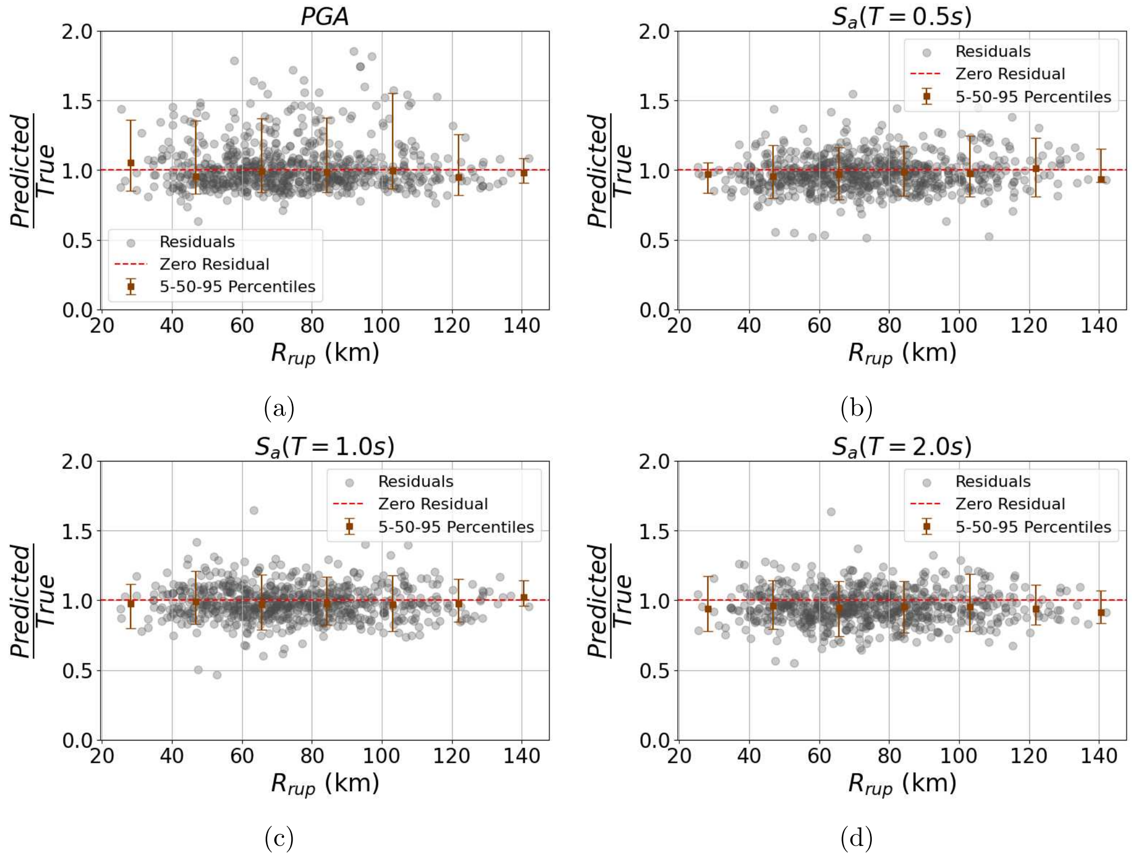

Figure 10: Residual plots of the SV-MEIM predictions for: (a) PGA, (b) $S_a(T = 0.5s)$, (c) $S_a(T = 1.0s)$, and (d) $S_a(T = 2.0s)$

To further evaluate the predictive performance and consistency of the SV-MEIM model, residual plots are analysed, as shown in Figure 10. These plots provide insight into the model's accuracy across different R_{rup} and periods. Since the sampled dataset only contains 871 number of earthquake events of ¡10 distinct M values, the residuals are only compared against distance, R_{rup}, to check for biases.

Figure 10 displays residual plots for PGA and selected S_a periods, where the residuals represent the ratio between the predicted and true values at seismic stations. An optimal model should produce residuals that are symmetrically distributed around the zero residual line, or also known as the unity line, indicating unbiased predictions. The results show that, for most cases, the residuals exhibit a balanced distribution with no significant skewness in relation to distance R_{rup}. However, it is generally observed that for the shorter periods the variance of residuals tends to be higher than the longer periods. This deviation suggests that the model tends to have a lower accuracy on S_a at shorter periods. The presence of higher variability at short period S_a values highlights the challenge of capturing non-linear ground motion characteristics effectively, where noise can more easily skew recording stations, causing inaccuracies in the data.

These visual analyses provide valuable diagnostic insights into the model's predictive capabilities. The residual plots help identify systematic biases, particularly in the prediction of extreme S_a. Based on these observations, further refinements can be explored, such as better datasets, residual correction techniques, or hyperparameter optimization. Enhancing the model's ability to capture extreme ground motion values and reducing uncertainty in short-period predictions would further improve its robustness for seismic hazard assessment and real-world deployment.

5.4 Case Study Analysis in Taiwan

The predictive performance of the SV-MEIM model is further analysed by using a case study event of $M = 6.3$ recorded in Taiwan. The selected case study event was chosen based on its frequency and representation within the seismic database, ensuring a well-distributed dataset for testing. This event was particularly withheld (belongs to the test set) during the training phase of the SV-MEIM. This approach ensures that the model's predictive capability is evaluated on an entirely unseen earthquake event.

Figure 11 presents the three-dimensional terrain-based heatmap (shakemap) mapped by the SV-MEIM model. The visualized IMs include PGA and $S_a(T)$ at different periods ($T = 0.5s, 1.0s, 2.0s$), enabling a comprehensive assessment of the seismic IMs across the region. The shakemap highlights both recorded and interpolated regions, capturing spatial variations in ground motion intensity, including areas lacking direct sensor measurements.

The triangular markers correspond to observed values at seismic stations, while the underlying heatmap represents model-predicted values interpolated across the entire terrain. The degree of alignment between a station marker's colour and the surrounding terrain indicates the model's accuracy in capturing spatial dependencies, with closer matches signifying higher predictive reliability. The results demonstrate that SV-MEIM effectively generalizes to unseen seismic events, with minimal discrepancies between recorded and predicted IMs at the sensored locations. For the unsensored location, the model non-linearly interpolates the IMs, thereby increasing the spatial resolution of hazard assessments.

Figure 11a illustrates the predicted and observed PGA distributions. The heatmap shows localized high-PGA zones near the earthquake epicentre and along major fault structures, consistent with strong ground motion attenuation patterns [24]. While the model captures broad PGA patterns accurately, minor discrepancies near station-dense regions observing high PGA may indicate complex near-surface effects not fully represented in the input features [62]. The $S_a(T = 0.5s)$ distribution exhibits similar spatial trends to PGA, given its sensitivity to high-frequency shaking [6]. However, slightly broader spatial dispersion of shaking intensity is observed, particularly in sedimentary basin regions of Taiwan [63]. The model's predictions align well with observed station values in most regions.

In Figure 11b, the $S_a(T = 1.0s)$ and $S_a(T = 2.0s)$ heatmaps present a more regionally smoothed intensity pattern compared to PGA and $S_a(T = 0.5s)$. This behaviour aligns with the longer-period characteristics of ground motion, where seismic waves experience lower attenuation and influence a broader area [64]. Notably, regions near the epicentre exhibit sustained moderate-to-high shaking, indicative of rupture directivity effects, where fault orientation and slip direction may concentrate energy in specific regions [65]. The SV-MEIM model effectively captures these trends, demonstrating strong generalization in areas without sensor coverage.

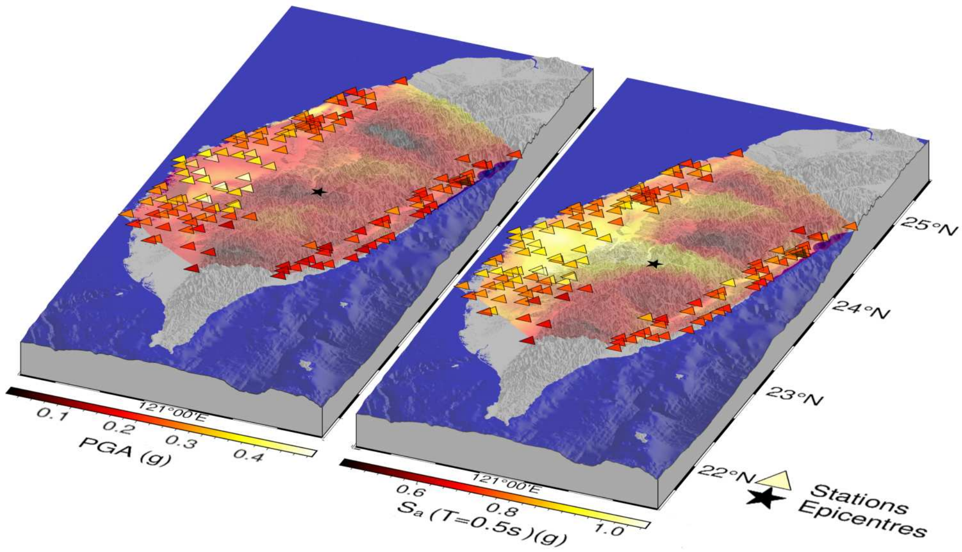

(a)

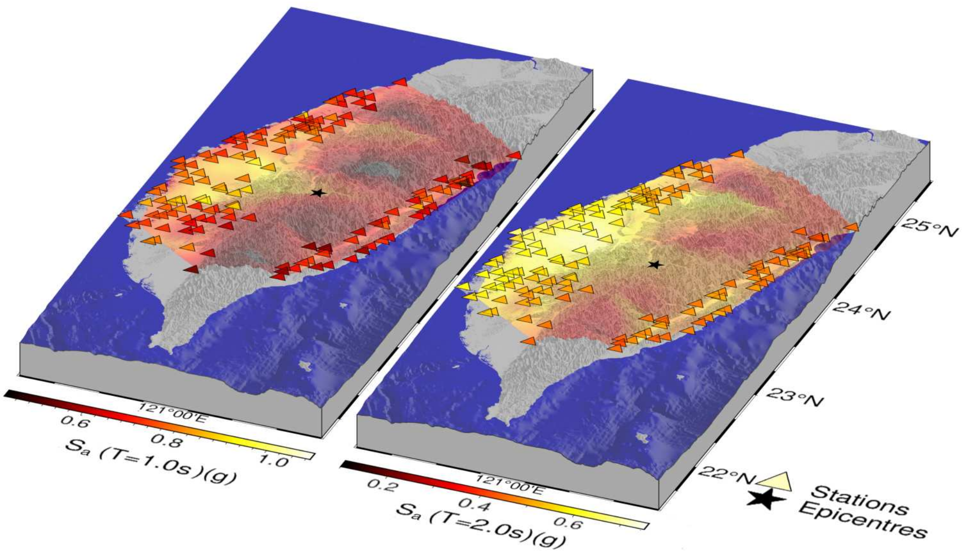

(b)

Figure 11: (a) Predicted heatmaps vs true records at stations for $M = 6.3$ event in Taiwan for PGA and $S_a(T = 0.5s)$; (b) Predicted heatmaps vs true records at stations for $M = 6.3$ event in Taiwan for $S_a(T = 1.0s)$ and $S_a(T = 2.0s)$

For $S_a(T = 2.0s)$, the heatmap reflects long-period shaking effects, which are critical for assessing seismic impacts on mid-rise and high-rise structures [66]. The spatial distribution reveals lower-frequency amplification in sedimentary basins and alluvial deposits, aligning with expected site resonance phenomena [67]. While the overall patterns remain consistent with observed station values, localized deviations in long-period response suggest that additional geotechnical input parameters (e.g., basin depth, V_{s30} variations) could further refine model accuracy in certain regions [68].

The incorporation of graph-based interpolation ensures that SV-MEIM accounts for spatial correlations in seismic wave propagation, even in areas with limited station coverage. Unlike traditional interpolation methods, this model also incorporates the underlying geophysical constraints such as soil properties and fault proximity and could be easily tuned to add more features.

6 Conclusion

This study addresses the challenge of predicting earthquake-induced ground motion IMs in regions lacking direct seismic observations. The proposed SV-MEIM (i.e., spatio-vectorial model for estimating earthquake intensity measures) integrates GNNs with a novel exponential transformation of IMs to capture both spatial correlations and cross-IM dependencies. Unlike traditional GMMs that rely on empirical regression or physics-based simulations, SV-MEIM provides a data-driven approach capable of dynamically learning non-linear spatial relationships between seismic stations while preserving the underlying physics of ground motion attenuation.

The graph-based architecture enables the estimation of IMs at unsensored locations, increasing the spatial granularity of ground motion fields beyond what is possible with classical interpolation-based methods. The introduction of GAT blocks further enhances model interpretability by prioritizing critical station interactions in the learning process.

Evaluation on the Taiwan case study demonstrated the model's capability to predict spatially distributed IMs across complex terrain with high fidelity. The heatmaps revealed that SV-MEIM effectively captured the attenuation and amplification effects in different geological regions, particularly in sedimentary basins where ground motion amplification is prominent. The model showed strong agreement with observed station values for PGA and mid-to-long period S_a ($S_a(T > 0.5s)$), accurately reflecting regional shaking patterns. However, analysis of residuals indicated higher variance at very short periods ($S_a(T = 0.1s)$), where high-frequency seismic waves are more susceptible to site-specific soil effects and broadband scattering phenomena. The model's performance in these cases suggests the need for further refinement, particularly in incorporating site response effects, nonlinear soil behaviour, and frequency-dependent damping mechanisms to improve generalization across all IM periods.

Future work can explore several key areas for refinement: (1) incorporating domain-specific constraints into the loss function, (2) developing hybrid models that integrate physics-informed graph-based learning, and (3) expanding the dataset through synthetic augmentation methods to mitigate data sparsity in under-monitored regions.

A major application of SV-MEIM is its potential integration into real-time seismic hazard assessment frameworks, such as ShakeMaps [7], which currently rely on kriging-based interpolation and empirical GMMs. The proposed SV-MEIM model offers a machine learning alternative that can dynamically adapt to new seismic events in near real-time, thereby improving the accuracy of post-earthquake response measures. Furthermore, SV-MEIM has broader implications in infrastructure resilience planning, structural fragility analysis, and earthquake risk mitigation strategies.

References

[1] U.S. Geological Survey. Understanding earthquakes and their impact. *USGS Publications*, 2021.

[2] Sinan Akkar and David M. Boore. Ground-motion prediction equations for global applications. *Bulletin of the Seismological Society of America*, 104(1):247–263, 2014.

[3] David M. Boore and Julian J. Bommer. Processing of strong-motion accelerograms: Needs, options and consequences. *Soil Dynamics and Earthquake Engineering*, 25:93–115, 2005.

[4] Andrew Coburn and Robin Spence. *Earthquake Protection.* John Wiley & Sons, 2004.

[5] Amr S. Elnashai and Luigi Di Sarno. *Fundamentals of Earthquake Engineering: From Source to Fragility.* Wiley, 2nd edition, 2015.

[6] Brian S.-J. Chiou and Robert R. Youngs. An nga model for the average horizontal component of peak ground motion and response spectra. *Earthquake Spectra*, 24(1):173–215, 2008.

[7] C. B. Worden and D. J. Wald. Shakemap ground motion mapping. *Encyclopedia of Complexity and Systems Science*, pages 8259–8272, 2010.

[8] Richard M. Allen. Earthquake early warning systems: Current status and perspectives. *Annual Review of Earth and Planetary Sciences*, 37:385–409, 2009.

[9] Georgianne Cua and Thomas H. Heaton. The virtual seismologist (vs) method: A bayesian approach to earthquake early warning. *Geophysical Research Abstracts*, 9:09242, 2007.

[10] Richard M. Allen and Diego Melgar. Earthquake early warning: Advances, scientific challenges, and societal needs. *Annual Review of Earth and Planetary Sciences*, 40:387–413, 2012.

[11] United Nations Office for Disaster Risk Reduction (UNDRR). Global assessment report on disaster risk reduction, 2019. Accessed: 2024-02-24.

[12] Charles K. Huyck and Benjamin J. Adams. Emergency response and recovery using remote sensing technology. *Disasters*, 30(2):179–193, 2006.

[13] Katsuichiro Goda and Jiandong Ren. Seismic risk assessment: Methods and applications. *Earthquake Engineering and Structural Dynamics*, 44(12):2065–2085, 2015.

[14] Keith A. Porter. How engineers can prepare for the next big earthquake. *Civil Engineering Magazine*, 88(7):46–53, 2018.

[15] Adam T. Ringler, Robert E. Anthony, and Austin A. Holland. Cost and performance trade-offs in deploying seismic stations for earthquake monitoring. *Seismological Research Letters*, 89(6):2310–2318, 2018.

[16] John F. Clinton, Thomas H. Heaton, and Egill Hauksson. The need for operational earthquake forecasting and seismic monitoring: Costs and benefits. *Seismological Research Letters*, 82(4):493–500, 2011.

[17] Egill Hauksson, Peter M. Shearer, and Guohui Lin. Southern california seismic network: Its role in earthquake hazard assessment and emergency response. *Seismological Research Letters*, 77(6):697–703, 2006.

[18] Julian J. Bommer and Norman A. Abrahamson. Why do modern probabilistic seismic-hazard analyses often lead to increased hazard estimates? *Bulletin of the Seismological Society of America*, 96(6):1967–1977, 2006.

[19] John Douglas. Earthquake ground motion estimation using strong-motion records: A review of predictive equations (empirical ground motion models). *Earth-Science Reviews*, 61(1–2):43–104, 2003.

[20] Katsuichiro Goda and Hao Hong. Spatial correlation of peak ground motions and response spectra. *Bulletin of the Seismological Society of America*, 100(3):939–953, 2010.

[21] Gail M Atkinson and David M Boore. Earthquake ground-motion prediction equations for eastern north america. *Bulletin of the seismological society of America*, 96(6):2181–2205, 2006.

[22] Kenneth W. Campbell and Yousef Bozorgnia. Nga-west2 ground motion model for the average horizontal components of pga, pgv, and 5 *Earthquake Spectra*, 30:1087–1114, 2014.

[23] Brian S.J. Chiou and Robert R. Youngs. Update of the chiou and youngs nga model for the average horizontal component of peak ground motion and response spectra. *Earthquake Spectra*, 30:1117–1153, 2014.

[24] Norman A. Abrahamson, Walter J. Silva, and Ronnie Kamai. Summary of the ask14 ground motion relation for active crustal regions. *Earthquake Spectra*, 30:1025–1055, 2014.

[25] Christopher R Vetter, Alexandros A Taflanidis, and George P Mavroeidis. Tuning of stochastic ground motion models for compatibility with ground motion prediction equations. *Earthquake Engineering & Structural Dynamics*, 45(6):893–912, 2016.

[26] Lucy A. Atik and Norman A. Abrahamson. Variability of ground-motion prediction models and its effects on seismic hazard analysis. *Earthquake Spectra*, 26(3):533–552, 2010.

[27] HP Hong, Y Zhang, and Katsuichiro Goda. Effect of spatial correlation on estimated ground-motion prediction equations. *Bulletin of the Seismological Society of America*, 99(2A):928–934, 2009.

[28] Samira Pouyanfar, Saad Sadiq, Yilin Yan, Haiman Tian, Yudong Tao, Maria Presa Reyes, Mei-Ling Shyu, Shu-Ching Chen, and Sundaraja S Iyengar. A survey on deep learning: Algorithms, techniques, and applications. *ACM computing surveys (CSUR)*, 51(5):1–36, 2018.

[29] Jawad Fayaz, Rodrigo Astroza, Claudio Angione, and Miguel Medalla. Data-driven analysis of crustal and subduction seismic environments using interpretation of deep learning-based generalized ground motion models. *Expert Systems with Applications*, 238, 3 2024.

[30] J Dhanya and STG Raghukanth. Ground motion prediction model using artificial neural network. *Pure and Applied Geophysics*, 175:1035–1064, 2018.

[31] Wenyi Zhu, Peng Liu, and Zhenghui Wang. A review of deep learning applications in seismology. *Earth-Science Reviews*, 218:103673, 2021.

[32] Qingkai Kong, Daniel T. Trugman, and Zachary E. Ross. Machine learning in seismology: Turning data into insights. *Seismological Research Letters*, 91(3):2046–2061, 2020.

[33] S. Mostafa Mousavi, William L. Ellsworth, Weiqiang Zhu, and Gregory C. Beroza. Earthquake transformer—an attentive deep-learning model for simultaneous earthquake detection and phase picking. *Nature Communications*, 11:3952.

[34] Jawad Fayaz, Miguel Medalla, Pablo Torres-Rodas, and Carmine Galasso. A recurrent-neural-network-based generalized ground-motion model for the chilean subduction seismic environment. *Structural Safety*, 100:102282, 2023.

[35] Jawad Fayaz and Carmine Galasso. A generalized ground-motion model for consistent mainshock–aftershock intensity measures using successive recurrent neural networks. *Bulletin of Earthquake Engineering*, 20(12):6467–6486, 2022.

[36] J. Dhanya and S. T.G. Raghukanth. Ground motion prediction model using artificial neural network. *Pure and Applied Geophysics*, 175:1035–1064, 2018.

[37] Jawad Fayaz, Miguel Medalla, Pablo Torres-Rodas, and Carmine Galasso. A recurrent-neural-network-based generalized ground-motion model for the chilean subduction seismic environment. *Structural Safety*, 100:102282, 2023.

[38] Jawad Fayaz, Sarah Azar, Mayssa Dabaghi, and Farzin Zareian. An efficient algorithm to simulate hazard-targeted site-based synthetic ground motions. *Earthquake Spectra*, 37:876–902, 2021.

[39] Stefan Bloemheuvel, Jurgen van den Hoogen, Dario Jozinović, Alberto Michelini, and Martin Atzmueller. Graph neural networks for multivariate time series regression with application to seismic data. *International Journal of Data Science and Analytics*, 16(3):317–332, 2023.

[40] Xitong Zhang, Will Reichard-Flynn, Miao Zhang, Matthew Hirn, and Youzuo Lin. Spatiotemporal graph convolutional networks for earthquake source characterization. *Journal of Geophysical Research: Solid Earth*, 127(11):e2022JB024401, 2022.

[41] Petar Veličković, Guillem Cucurull, Arantxa Casanova, Adriana Romero, Pietro Lio, and Yoshua Bengio. Graph attention networks. *arXiv preprint arXiv:1710.10903*, 2017.

[42] Florian Cajori. *A History of Mathematical Notations.* Open Court Publishing Company, 1952.

[43] Timothy D Ancheta, Robert B Darragh, Jonathan P Stewart, Emel Seyhan, Walter J Silva, Brian S-J Chiou, Katie E Wooddell, Robert W Graves, Albert R Kottke, David M Boore, et al. Nga-west2 database. *Earthquake Spectra*, 30(3):989–1005, 2014.

[44] Maurice Power, Brian Chiou, Norman Abrahamson, Yousef Bozorgnia, Thomas Shantz, and Clifford Roblee. An overview of the nga project. *Earthquake spectra*, 24(1):3–21, 2008.

[45] David M. Boore, Jennie Watson-Lamprey, and Norman A. Abrahamson. Orientation-independent measures of ground motion. *Bulletin of the Seismological Society of America*, 96:1502–1511, 8 2006.

[46] Jawad Fayaz and Farzin Zareian. An efficient algorithm to simulate site-based ground motions that match a target spectrum. *Earthquake Engineering and Structural Dynamics*, 50(13):3532–3549, 2021.

[47] Stefan Bloemheuvel, Jurgen van den Hoogen, Dario Jozinović, Alberto Michelini, and Martin Atzmueller. Graph neural networks for multivariate time series regression with application to seismic data. *arXiv preprint arXiv:2201.00818*, 2022.

[48] Ian W McBrearty and Gregory C Beroza. Earthquake location and magnitude estimation with graph neural networks. *arXiv preprint arXiv:2203.05144*, 2022.

[49] Maosen Li, Siheng Chen, Ya Zhao, Ya Liu, Yanfeng Wang, and Qi Tian. Dynamic multiscale graph neural networks for 3d skeleton-based human motion prediction. In *Proceedings of the IEEE/CVF Conference on Computer Vision and Pattern Recognition*, pages 214–223, 2020.

[50] Michel Destrade. Seismic rayleigh waves on an exponentially graded, orthotropic half-space. *arXiv preprint arXiv:0711.4576*, 2007.

[51] Thomas M. Cover and Peter E. Hart. Nearest neighbor pattern classification. *IEEE Transactions on Information Theory*, 13(1):21–27, 1967.

[52] Gueorgi Kossinets, Jon Kleinberg, and Duncan Watts. The structure of information pathways in a social communication network. In *Proceedings of the 14th ACM SIGKDD international conference on Knowledge discovery and data mining*, pages 435–443, 2008.

[53] Nancy Marshall and Marvin D Glock. Comprehension of connected discourse: A study into the relationships between the structure of text and information recalled. *Reading Research Quarterly*, pages 10–56, 1978.

[54] Marco Baiesi and Maya Paczuski. Complex networks of earthquakes and aftershocks. *Nonlinear Processes in Geophysics*, 12(1):1–11, 2005.

[55] Arthur D Frankel. How does the ground shake? *Science*, 283(5410):2032–2033, 1999.

[56] John X Zhao and Hua Xu. A comparison of vs 30 and site period as site-effect parameters in response spectral ground-motion prediction equations. *Bulletin of the Seismological Society of America*, 103(1):1–18, 2013.

[57] Charles F Richter. An instrumental earthquake magnitude scale. *Bulletin of the seismological society of America*, 25(1):1–32, 1935.

[58] Ahmad Ali, Yanmin Zhu, and Muhammad Zakarya. Exploiting dynamic spatio-temporal graph convolutional neural networks for citywide traffic flows prediction. *Neural networks*, 145:233–247, 2022.

[59] Jin Fan, Ke Zhang, Yipan Huang, Yifei Zhu, and Baiping Chen. Parallel spatio-temporal attention-based tcn for multivariate time series prediction. *Neural Computing and Applications*, 35(18):13109–13118, 2023.

[60] Graeme Weatherill, S. R. Kotha, Laurentiu Danciu, S. Vilanova, and Fabrice Cotton. Modelling seismic ground motion and its uncertainty in different tectonic contexts:

challenges and application to the 2020 european seismic hazard model (eshm20). *Natural Hazards and Earth System Sciences*, 24:1795–1834, 2024.

[61] Victor C. Tsai and Greg Hirth. Elastic impact consequences for high-frequency earthquake ground motions. *Geophysical Research Letters*, 47(4):e2019GL086302, 2020.

[62] Jonathan P. Stewart, Kayhan Afshari, and Christine A. Goulet. Effects of near-surface geology on seismic ground motion. *Earthquake Spectra*, 33(1):113–127, 2017.

[63] Kuo-Liang Wen, Teng-Yi Chang, and Chung-Ming Lin. Seismic site effects and seismic zoning in taiwan. *Journal of Asian Earth Sciences*, 40:691–703, 2011.

[64] Robert W. Graves and Arben Pitarka. Simulation of ground motion for the 1994 northridge, california, earthquake using a hybrid approach. *Bulletin of the Seismological Society of America*, 101(4):1484–1502, 2011.

[65] Paul Spudich and Brian S. Chiou. Directivity in nga ground motion models. *Bulletin of the Seismological Society of America*, 89:1156–1170, 1999.

[66] Nicolas Luco and C. Allin Cornell. Structure-specific seismic hazard analysis for performance-based earthquake engineering. *Earthquake Spectra*, 18(1):131–162, 2002.

[67] Pierre-Yves Bard and Michel Bouchon. The effects of surface geology on seismic motion: A comprehensive review. *Bulletin of the Seismological Society of America*, 98(3):791–811, 2008.

[68] Eric M. Thompson, David J. Wald, and Charles B. Worden. A vs30 map for california with geologic and topographic constraints. *Bulletin of the Seismological Society of America*, 102(6):2345–2358, 2012.